Published in final edited form as:
Nat Struct Mol Biol. ; 19(4): 424–429. doi:10.1038/nsmb.2255.

A sensor-adaptor mechanism for enterovirus uncoating from structures of EV71

Xiangxi Wang[1], **Wei Peng**[1], **Jingshan Ren**[2], **Zhongyu Hu**[3], **Jiwei Xu**[1], **Zhiyong Lou**[4], **Xumei Li**[1], **Weidong Yin**[3], **Xinliang Shen**[3], **Claudine Porta**[2], **Thomas S. Walter**[2], **Gwyndaf Evans**[5], **Danny Axford**[5], **Robin Owen**[5], **David J. Rowlands**[6], **Junzhi Wang**[3], **David I. Stuart**[2,5], **Elizabeth E. Fry**[2], and **Zihe Rao**[1,4]

[1]National Laboratory of Macromolecules, Institute of Biophysics, Chinese Academy of Science, Beijing, 100101, China

[2]Division of Structural Biology, University of Oxford, The Henry Wellcome Building for Genomic Medicine, Headington, Oxford, UK

[3]National Institutes for Food and Drug Control, No. 2, TiantanXili, Beijing 100050, China

[4]Laboratory of Structural Biology, School of Medicine, Tsinghua University, Beijing, 100084, China

[5]Diamond Light Sources, Harwell Science and Innovation Campus, Didcot, OX11 0DE, UK

[6]Institute of Molecular and Cellular Biology and Astbury Centre for Structural Molecular Biology, Faculty of Biological Sciences, University of Leeds, Leeds, UK.

Abstract

Enterovirus 71 (EV71), a major agent of hand-foot-and-mouth disease in children, can cause severe central nervous system disease and mortality. At present no vaccine or antiviral therapy is available. We have determined high-resolution structures for the mature virus and natural empty particles. The structure of the mature virus is similar to that of other enteroviruses, whilst the empty particles are dramatically expanded, with notable fissures, resembling elusive enterovirus uncoating intermediates not previously characterized in atomic detail. Hydrophobic capsid pockets within the EV71 capsid are collapsed in this expanded particle, providing a detailed explanation of the mechanism for receptor-binding triggered virus uncoating. The results provide a paradigm for enterovirus uncoating, in which the VP1 GH loop acts as an adaptor-sensor for the attachment of cellular receptors, converting heterologous inputs to a generic uncoating mechanism, spotlighting novel points for therapeutic intervention.

Hand-foot-and-mouth disease (HFMD) is a serious public health threat across the Asia-Pacific region, as evidenced by the more than 1.7 million cases that were reported by the Chinese Ministry of Health in China during 2010. The dominant causative agent is EV71, a

Correspondence should be addressed to D.I.S. (dave@strubi.ox.ac.uk) or E.E.F (liz@strubi.ox.ac.uk) or J.W. (wangjz@nicpbp.org.cn) or Z.R. (raozh@xtal.tsinghua.edu.cn)..
X.W., W.P. and J.R. contributed equally to this work.

Author Contribution. JW, ZH, WY and XS prepared samples. XW, WP, XL, ZL, JX,JR, CP, TSW, EEF and DIS performed research, WP, XW, ZL JR, EEF and DIS analysed data and with DJR and ZR wrote the manuscript, in discussion with JW, ZH, WY and XS. All authors contributed to experimental design. Project supervision: ZR, DIS.

Accession codes. The coordinates and structure factors for formaldehyde inactivated full virus in two space groups, the empty particle at 100K and 21°C, and native full and empty viruses have been deposited with the RCSB under accession codes: 3VBF, 3VBH, 3VBO, 3VBR, 3VBS and 3VBU, respectively.

The authors declare no competing financial interest.

Europe PMC Funders Author Manuscripts

non-enveloped single-stranded RNA virus (genus *Enterovirus,* family *Picornaviridae*) closely related to Coxsackievirus A16, the other etiological agent of HFMD[1]. Whilst A16 infections are not usually serious, acute EV71 infections may cause severe neurological disease[2,3], leading to 905 deaths in China in 2010.

The icosahedral capsid of EV71 comprises 60 copies of four protein subunits, VP1-VP4. During assembly the P1 polyprotein is cleaved to yield VP0 (36KD), VP1 (32KD) and VP3 (27KD). The final cleavage of VP0 into VP2 (28KD) and VP4 (8KD), autocatalysed by viral RNA, forms the mature viral capsid[4,5], in which VP1-VP3 follow a pseudo T=3 arrangement and span the thickness of the capsid[6], whilst VP4 is located on the inside. Picornaviruses may also produce empty particles, which resemble the mature virus in structure and antigenicity, sediment at ~73S and comprise 60 copies of VP0, VP1 and VP3[4,7,8]. In-line with this, EV71 cultured in Vero cells for vaccine development produces two distinct types of particles[9]: highly infectious mature virions, composed of VP1-4 and RNA, and empty particles containing VP0, VP1 and VP3. Although 73S particles are no longer thought to be direct precursors of mature virions, they can function as reservoirs of capsid components[8,10,11], presumably following their dissociation into functional subunits. 73S particles are rather unstable, readily converting from D-type native antigenicity to a state with altered (C-type in the poliovirus nomenclature[12,13]) antigenic properties.

Structural studies have outlined the processes leading to cell infection by enteroviruses[14]. Cellular receptors attach to the virus, often binding in a canyon-like depression surrounding the 5-fold axis[15-17]. This triggers conformational changes in the virus, leading to the formation of an expanded intermediate with altered antigenic properties, which sediments at ~135S (*cf* ~160S for the mature virus)[18-20]. This conformational change (which can also be induced by environmental insults such as heating or low pH), leads to the externalisation of VP4 and the VP1 N termini[21,22], followed by extrusion of the viral genome into the cytoplasm of the target cell, to leave an ~80S empty particle[21]. From low-resolution data, the consensus view was that the viral RNA probably exited via a 5-fold axis channel[14], although recent studies suggest it exits near a 2-fold axis[23]. There remains a dearth of high-resolution structural detail to illuminate the molecular mechanisms underpinning this dynamic cell-entry process. We have determined structures of both inactivated and infectious EV71 virions, and of expanded natural empty particles closely resembling expanded enterovirus uncoating intermediates previously visualized by cryo-electron microscopy (cryo-EM)[24,25]. Our high-resolution analyses suggest a detailed molecular mechanism for the early stages of enterovirus uncoating.

Results

Characterization and structure determination

EV71 was isolated from a patient from Anhui, China, and cultivated in Vero cells. When required, virus was formaldehyde inactivated before being purified by centrifugation, ultrafiltration, PEG-precipitation and gel filtration (**Online Methods**). Unless otherwise stated analyses used inactivated virus. Two particle types were separated by ultracentrifugation (Supplementary Fig. 1) and characterized by SDS-PAGE and analytical ultracentrifugation (Supplementary Fig. 1) as mature virions, containing RNA and a full complement of proteins VP1-4 with a sedimentation coefficient of 150S, and 82S empty particles containing VP0, 1 and 3. The sedimentation coefficient of the empty particles is significantly greater than that of native antigenicity enterovirus empty particles (~73S), despite an earlier report that EV71 empty particles were smaller than virus[9]. Furthermore a monoclonal antibody recognizes the virus but not the empty particle, demonstrating differences in antigenicity between the two particles (Supplementary Fig. 2). These results, and the considerable thermal stability of the empty particles (Supplementary Fig. 2) suggest

that native antigenicity EV71 empty particles rapidly and spontaneously reconfigure to the altered state that we characterize here. Diffraction data were collected from small crystals primarily at 21°C directly from the crystallization plates (*in situ*), avoiding problems of harvesting and cryoprotecting the fragile crystals. We believe this represents the first report of a virus structure determination using such a method. The structure of mature inactivated virus was solved in two spacegroups (*R*32 and *I*23) with 21°C data merged from multiple crystals. For the empty particle, a high-resolution dataset was collected at 100K, and a lower resolution data set at 21°C. This provided reliable atomic models at resolutions of 2.3, 2.6, 2.9 and 3.8 Å respectively for two independent structure determinations each for full virus and empty particles (see Table 1, **Online Methods** and Supplementary Fig. 3). Although particles were formaldehyde inactivated (Supplementary Fig. 1) there was no evidence in the electron density for systematic specific covalent cross-linking and subsequent structure determinations of non-inactivated particles (Table 1) showed that inactivation did not perturb the structures. Unless otherwise stated descriptions below apply to all the structures of that particle type.

Structure of the mature virus

Mature EV71 is well-ordered apart from a few disordered residues in VP4 and VP2 (Fig. 1) and is most similar to Bovine enterovirus (BEV1) (Supplementary Fig. 4 presents structure-based sequence alignments and phlyogenies**)**. The inner capsid surface is distinct from other enteroviruses (Supplementary Fig. 4). Residues 1-28 of VP1 usually proceed towards the 5-fold axis but in EV71 veer across the protomer, presenting a short helix (residues 5-9) underneath the αA helices of VP2, adjacent to the icosahedral 2-fold axes. Residues 14-31 of VP4 form a loose spiral beneath VP1 rather than lying under the adjacent biological protomer. One RNA base stacks against VP2 Trp38 (as in other enteroviruses[26]) and another may interact with VP1 Gln30 and VP3 Gln48. On the outside of the particle the VP1 BC, DE and HI loops are flattened away from the 5-fold axis (as in BEV1), with residues 96-102 (BC loop) and 208-222 (GH loop) being the most exposed (Fig. 1c). Part of the VP2 EF loop (128-148) is unusually extended and surface dominant whilst the remainder (151-172) is shorter than usual and less accessible. Exposed residues in VP3 include 58-69 and 173-190 (Supplementary Fig. 5).

An expanded natural empty particle

The EV71 empty particles are markedly larger than any other picornavirus particle characterized crystallographically (Fig. 1b), the rms capsid radius increasing from 132 Å for the mature virion to 139 Å for the empty particle. Whilst cooling virus particles to 100K often induces modest isotopic shrinkage (~1%), in this case both the 293K and 100K empty particles are ~4% larger than the 293K mature virus and moreover the 100K particles are not icosahedral. Thus refinement imposing icosahedral symmetry stuck at an R-factor of 30%, but improved dramatically when this was relaxed. Cryo-cooling distorts the particle, pushing Cαs in the crystal contact region ~1.3 Å towards the particle centre (the 293K and 100K structures are otherwise essentially identical) (Supplementary Fig. 5). Such deviations from icosahedral symmetry have never been observed in mature viruses and reflect the extreme flexibility of these expanded particles, explaining why it has proved difficult to visualize them at high-resolution. The expansion of the empty particles reflects tectonic movements within the particle, which partially separate the protomeric units, disordering over 70,000 protein atoms per particle, and forming perforations at the icosahedral 2-fold axes and at the base of the canyon (Fig. 2, a and b). Several external loops, which nestle at the junction of polypeptide chains, become disordered, including five residues at the C-terminus of VP2 and residues 211-217 of the GH loop of VP1, whilst the VP3 GH loop undergoes a major conformational switch, residues 170-192 converting from loop and helix to almost a β-hairpin upon expansion and become less ordered (for residues 174-190 B-factors exceed

100Å^2) (Supplementary Fig. 5). On the inside of the particle the internal festoon comprising the N-terminal 72 residues of VP1 and the first 81 residues of VP0 vanishes from the electron density (see Fig. 1). Overall surface properties are appreciably altered, the interactions that hold the particle together are dramatically reduced (Supplementary Table 1), and the expanded particle is thinned to 20Å from 23Å in the mature virus (Fig. 2c). The core structures of the individual polypeptides are less affected (Fig. 1c), although some important rearrangements occur.

Enteroviruses adopt two fundamental configurations

The ~4% expansion of the EV71 82S empty particle is similar to that seen for poliovirus 135S and 80S uncoating intermediates[27], and the latter has similar hydrodynamic properties. Cryo-EM analyses revealed that the poliovirus 135S and 80S particles are structurally similar to each other[27] (although the latter has shed the viral genome), and are reconfigured compared to the mature virus[24,25]. We used VEDA[28] to compare the EV71 expanded particle with the poliovirus particles. Remarkably the EV71 particle fitted the poliovirus 135S and 80S electron densities as well as did the polio structure previously modeled into this density (Fig. 2d-g). Thus at low resolution the EV71 expanded assembly by-product is indistinguishable from poliovirus uncoating intermediates. Furthermore we find that heat treatment of mature EV71 particles (using a protocol similar to that which produces 135S poliovirus particles) converts them to particles which crystallize isomorphously with 82S immature particles (data not shown). It seems that the plethora of enterovirus particles formed during assembly and uncoating possess only two fundamental configurations, both now defined in atomic detail. The mature virus particle, which is rigid and rendered more stable by cleavage of VP0, is generally converted to the second, expanded, configuration following cell attachment. The remarkably flexible expanded particle can adopt subtly different conformations during the process of uncoating as it progresses from a 135S to 80S form[25], but can also arise from the conversion of unstable VP0 containing natural empty particles, as seen for poliovirus[10,11] and now EV71.

Mechanics of particle expansion

Particle expansion is accompanied by a 5.4° counter-clockwise rotation of the protomeric building block (VP1, VP0, VP3), which pivots about the corner of VP3 at the icosahedral 3-fold axis (Fig. 3a). This screw-like movement moves VP1 and the underlying VP3 hub away from the particle centre by up to 7Å and pulls VP0 away from the 2-fold axis by 5Å, opening up perforations. In addition to large-scale disordering (described above), small-scale changes occur on the edges of the protomers (Fig. 3, b and c). The separation at the 2-fold axes rips apart the αA helices of adjacent VP2 subunits which form a key interaction stabilizing the mature virus (Fig. 3, d-g). These helices are capped by side-chains that compensate the helix dipole. In the expanded capsid the C-terminal cap (Arg249) becomes poorly ordered, suggesting mechanical strain (the five C-terminal residues beyond it are disordered). Within the protomeric unit, a 7.5° rotation and 1.4 Å translation of the 5-fold proximal end of the VP1 β-barrel, which is jack-knifed upwards in the mature virus (Fig. 3c), straightens the protomer. and moves the GH loop, H strand, CD loop and residues ~262-280 beyond strand I of VP1. The trigger for protomer extension appears to be changes centered on a pocket within the VP1 β-barrel.

Mature EV71, in common with other enteroviruses, possesses a hydrophobic pocket that penetrates from the surface deep into the interior of the VP1 β-barrel, underlying a canyon-like surface depression[16] and harbouring a natural lipid (possibly sphingosine, as seen in poliovirus[29], Fig. 4 and Supplementary Fig. 3). Interestingly the only visible difference between active and inactivated particles is that in the active virus the occupancy of the ‘pocket-factor’ is reduced (to ~0.5 compared to ~1 in the inactive virus, Supplementary Fig.

6). This suggests that formaldehyde treatment might rigidify the particle, inhibiting the release of the pocket-factor, and presumably contributing to inactivation since pocket-factor release appears to be required for the initiation of uncoating[30,31] (potential antivirals have been discovered that replace natural lipids and inhibit uncoating[31,32]). Indeed inactivation does not appear to cross-link the majority of the capsid proteins either to each other or to viral RNA (Supplementary Fig. 1), but presumably operates by the cooperative effect of a small number of cross-links made in each virus particle. Until now, empty pockets observed in enteroviruses[16,26,33,34], have been largely open (such that a pocket-factor might bind without appreciable structural change). In contrast the EV71 expanded particle pocket is not only empty, but has collapsed to a state incompatible with pocket-factor binding (from 1,000 $Å^3$ in the mature virus, to 580 $Å^3$, program Volumes, R. Esnouf, unpublished). This arises from small conformational changes in the external walls of the pocket. (Fig. 4b,c, Supplementary Figs 4 & 6). The largest movement of the polypeptide backbone is in residues 230-233 at the end of the GH loop and start of strand H, where Cα movements reach ~2.5 Å and two side-chains reposition to ablate the pocket: Met230 moves ~5 Å and the phenol ring of Phe233 swings ~90° (Fig. 4c). Interestingly this portion of chain, which we term the *adaptor-sensor*, is directly downstream of a region of the GH loop which is external and structurally quite variable in poliovirus (Supplementary Figure 6). This variability may reflect an unknown biological function or may simply facilitate the expansion switch. Rearrangement of the adaptor-sensor shifts the walls of the canyon to straighten the VP1 core. Furthermore, in mature particles this region directly contacts the C-terminal residues of VP2 including the Arg249 cap stabilizing the VP2 αA helix. On conversion to the expanded particle this region becomes distorted and partly disordered, perhaps introducing strain that facilitates the separation of the VP2 αA helices to complete particle expansion. Indeed, a capping arginine is conserved in all enteroviruses (and cardioviruses) but absent from the less stable aphthoviruses (Supplementary Fig. 4). In summary, closure of the VP1 pocket initiates enterovirus uncoating via a mechanical connection to the pentamer interface.

Antigenicity and receptor engagement

Residues 210-220 of VP1, preceding the adaptor-sensor, are part of an important neutralising epitope of EV71[35]. They lie on the capsid surface, alongside the VP2 EF loop (residues 136-150), to form a single epitope[35,36], however residues 211-217 become disordered upon particle expansion, probably explaining the loss of immunogenicity reported previously[9] and seen by us (Supplementary Fig. 2). The surface charge of the virion is consistent with initial cell attachment occurring via a sugar moeity (Supplementary Fig. 7), however whilst three glycoproteins have been suggested as receptors[37-39], their binding sites on EV71 are unknown. Nevertheless enterovirus receptors frequently attach at the canyon[40] and mapping cryo-EM enterovirus-receptor complexes (PDB codes 1NN8[41], 1Z7Z[42], 1AYN[43], 1MEC[44]) onto mature EV71, reveals that they make similar contacts with the canyon walls at the adaptor-sensor region. We propose that full engagement of receptor with the adaptor-sensor switches its conformation to a high receptor-affinity form (reported, *e.g.* for poliovirus[45]), triggering expulsion of the pocket-factor and conversion to the expanded particle.

Discussion

The mechanism by which the RNA genome is productively released from picornaviruses has long been the subject of speculation[16,23,25,46]. Whilst details will vary, the process is probably fundamentally similar for all enteroviruses. RNA release in poliovirus is preceded by the egress of the VP1 N-terminus and VP4[21], which may associate to form a channel through the membrane allowing the safe transfer of the viral genome to the cell cytoplasm. Candidates for membrane association and channel formation are the myristate group at the

N-terminus of VP4[47] and a region at the N-terminus of VP1 proposed to form an amphipathic helix[48]. It had been assumed that a 5-fold channel would be formed to release these regions[46], however recent studies suggest instead that VP1 at least leaves at the base of the canyon or at a 2-fold axis[23,24,49]. We have defined a channel at the base of the canyon (7×9 Å in size) and a larger (8×25 Å) opening at the 2-fold axis (Fig. 2b), either of which would allow egress of a polypeptide chain whilst the larger might allow the exit of RNA. Interestingly, in the mature EV71 virus the N-terminal region of VP1 lies at the 2-fold axis, rather than close to the 5-fold axis, perhaps presenting a snapshot of a structural rearrangement that precedes VP1 release in other enteroviruses. Indeed in the expanded particle both VP4 and the VP1 N-terminus are disordered, and possibly already partly extruded. During exit of the RNA through one of the openings we observe, less structured regions of the ssRNA genome might be transiently unwound through interactions with the inner surface of the capsid, but the considerable secondary structure at the termini of picornavirus genomes suggests that strain would be required to initiate RNA egress, perhaps accounting for the fact that the RNA does not spontaneously exit 135S particles. Such strain could probably be accommodated by the flexibility of the expanded particle which could allow the two openings to merge by breaking the single weak link between them (Fig. 3 e & g). Interestingly flexing of this region would render a conserved VP3 sequence (PPGxxxPxxR[50], reminiscent of a protein binding motif) accessible on the inside of the particle. This motif may be involved in picornavirus assembly or uncoating.

Our results have two lessons for vaccine production, (i) formaldehyde inactivation leaves the structure, and hence antigenicity, of EV71 essentially unchanged, (ii) when grown in Vero cells, this strain of EV71 produces large amounts of antigenically altered particles, which will, at best, dilute the useful portion of a vaccine. More broadly our results, with those of others, show that the key structural transitions of enteroviruses are based on just two fundamental states with very different physico-chemical and antigenic properties matched to their distinct roles in the virus lifecycle. Atomic level descriptions of these states allow us to propose a mechanism by which receptor binding triggers virus uncoating, and to highlight points where we might attempt to modulate the switch between the two states, using either small molecules or, for recombinant vaccine production, mutations of the virus. One such point is the well-studied VP1 hydrophobic pocket[31]. A second is the pair of VP2 αA helices, which are torn apart during expansion - mutations that weaken the link from the adaptor-sensor to this point might be useful in providing stabilized vaccines. Furthermore key amino acid residues in the proposed uncoating mechanism are conserved beyond the enteroviruses (Supplementary Fig. 4), suggesting that by targeting elements of the mechanism that are common to other picornavirus genera it may be possible to develop generic therapies against a number of viruses which are serious threats to health.

Supplementary Material

Refer to Web version on PubMed Central for supplementary material.

Acknowledgments

We thank Sinovac Biotech Ltd. and the China National Biotech Group for providing virus samples, Dr Robert Gilbert for assistance with analytical unltracentrifugation, Robert Esnouf for help with pocket analysis, Jonathan Grimes for various help, especially with VEDA, and Abhay Kotecha for assistance with Diamond data collection. We also thank the Photon Factory, Japan and the NSRL, China. Work was supported by the National Major Project of Infectious Disease, the Ministry of Science and Technology 973 Project (grant no. 2007CB914304). DIS, EEF & TSW are supported by the UK Medical Research Council, JR by the Wellcome Trust and CP by DEFRA.

APPENDIX

ONLINE METHODS

Particle production and purification

EV71 (genotype C4), isolated from Fuyang, Anhui Province, China, was used to infect Vero cells at 10^7 $TCID_{50}$. Virus was harvested 5-6 days post infection, inactivated by incubation with 100 μgmL^{-1} formaldehyde at 37°C for 3 days, centrifuged to remove cell debris, ultrafiltered, PEG precipitated and subjected to gel filtration. These stages were performed by Sinovac Biotech Ltd and the China National Biotech Group. Crude EV71 concentrate (~0.6 mg in 600 μL PBS pH7.4) was loaded onto a 15%-45% (w/v) sucrose density gradient and centrifuged at 103,614g for 3.5h in an SW41 rotor at 4°C. Two sets of fractions were collected and dialyzed against PBS buffer (Supplementary Fig. 1), one comprised empty particles (containing no RNA), the other virions. SDS-PAGE analysis used a NuPAGE 4-12% Bis-Tris Gel (Invitrogen) (Supplementary Fig. 1).

Analytical ultracentrifugation

The sedimentation coefficients for both types of particles were determined using a Beckman XL-I analytical ultracentrifuge at 4°C (Supplementary Fig, 1).

D6 Fab purification and EV71 immunogenicity

Anti-EV71 monoclonal antibody (mAb) D6 was supplied by Sinovac. Fab fragments were generated (Pierce@FAB preparation kit, Thermo Scientific), dialyzed against 20mM acetate pH5.0 at 4 °C, loaded on a Mono S column (GE heathcare), and eluted using a 0-500 mM NaCl gradient. The main peak was collected and dialyzed into PBS buffer. The pure Fab was incubated with the semi-purified EV71 containing empty and full particles (at a ratio of ~240 Fab molecules per EV71 virion) at 4°C for 12h. The mixture was loaded onto a 15%-45% (w/v) sucrose density gradient and centrifuged at 103,614g for 3.5h using a SW41 rotor at 4°C (Supplementary Fig. 2).

Thermofluor assay

Thermofluor experiments were performed with an MX3005p RT-PCR instrument (Agilent). SYTO9 and SYPROred (both Invitrogen) were used as fluorescent probes to detect the presence of RNA and the exposed hydrophobic regions of proteins respectively. 50 μL reactions were set up in a thin-walled PCR plate (Agilent), containing 0.5-1.0 μg of either the virus or empty particles, 5 μM SYTO9 and 3X SYPROred in PBS pH7.4 and ramped from 25-99 °C with fluorescence recorded in triplicate at 1 °C intervals. The melting temperature, T_m, was taken as the minimum of the negative first derivative of the denaturation curve (Supplementary Fig. 2).

Crystallization

Crystallization used nano-litre vapour diffusion in Greiner CrystalQuick™X plates[52]. Purified particles were concentrated to 2mg/mL in PBS pH7.4. Crystal Screen1 (Hampton Research) condition 13 (30% PEG400, 0.2 M tri-Sodium Citrate, 0.1 M Tris.HCl pH 8.5) gave small irregular crystals. Since standard optimization techniques failed 20% of this condition was added to the virus solution, and then equilibrated against alternative reservoirs: the SaltRx screen solutions (Hampton Research, USA). Crystals emerged in over half of the 96 conditions with maximum size of 0.15×0.15×0.02 mm^3, in three crystal morphologies: rhomboid plates, cubic and triangular prisms. Crystals of empty particles grew in two conditions (i) 200 mM Ammonium phosphate monobasic, 24% (v/v) Isopropanol and 100 mM sodium cacodylate (pH 6.5); and (ii) 1.4 M sodium acetate and 0.1

M sodium cacodylate (pH 6.5). The crystallisation conditions were similar for inactivated and non-inactivated virus.

Structure determination

Room temperature diffraction data were collected from crystals in crystallization plates (*in situ*), a method developed at beamline I24, Diamond (Axford *et al.* to be published). Diffraction images of 0.05° or 0.1° oscillation were recorded on a Pilatus6M detector using a 0.02×0.02 mm^2 or 0.05×0.05 mm^2 beam according to crystal size. The X-ray beam was focused downstream from the crystal. Using 0.05s exposure time and 100% beam transmission, typically 6 to 10 useful images could be collected from one position on a crystal (up to 6 positions for larger crystals). Data for the EV71 inactivated full particles were collected from the rhomboid plates and cubic crystals (space groups *R*32 and *I*23, respectively, Table 1). Room temperature data were also collected for the empty EV71 inactivated particles to 3.8 Å resolution. The data were weak (by the usual current standards of macromolecular crystallography), and this is reflected in the poor merging R-factors. Subsequently data were collected, to lower resolution, from non-inactivated full and empty particles (Table 1).

Cryo-cooled (100K) data for crystals of empty EV71 particles were measured using 0.1° 1s exposure oscillations. Crystals were soaked for 20 minutes in a cryoprotectant solution (80% (v/v) reservoir solution and 20% (v/v) glycerol) before being plunged into liquid nitrogen.

Data were analysed using HKL2000[53]. The structures of both empty and full inactivated particles were determined by molecular replacement. For the empty particle ($P4_232$, $a=b=c$=353.1 Å (100K data)) there is an icosahedral pentamer in the crystallographic asymmetric unit. For the full virus (*R*32 $a=b$=330.0 Å and c=748.4 Å and *I*23, $a=b=c$=600.1 Å) there are 2 and 4 pentamers in the asymmetric unit, respectively. Molecular replacement used BEV (PDB ID:1BEV) as the search molecule (most orientation and positional parameters were defined by the alignment of icosahedral and crystallographic symmetry axes). For the *I*23 crystals, the centre of the virus is at (¼,¼,¼). In each case, the crystallographic asymmetric unit was rigid-body refined. Cyclic positional, simulated annealing and B-factor refinement used strict NCS constraints with CNS[54]. Averaging used GAP (DIS, J Grimes & J Diprose, unpublished) and models were rebuilt with COOT[55]. Refinement of the empty particle cryo-structure stuck at an R-factor of 0.30. Rigid-body refinement of individual protomers (breaking the icosahedral symmetry), reduced the R-factor to 0.25 (all data to 2.88 Å). Inspection revealed that at the crystallographic contacts, the structure was squashed 1.3 Å inwards, presumably due to crystal freezing. BUSTER[56] refinement using NCS restraints gave an R-factor of 0.187. Recalculated NCS matrices were used as constraints with CNS, resulting in the final structure (Table 1). The non-inactivated structures were isomorphous with the inactivated structures and were refined directly from those structures, using strict NCS constraints in CNS. Models were verified with PROCHECK[57] (Table 1). Structural comparisons used SHP[51]. Unless otherwise noted structural figures were prepared with PyMol[58].

References

1. Brown BA, Pallansch MA. Complete nucleotide sequence of enterovirus 71 is distinct from poliovirus. Virus Res. 1995; 39:195–205. [PubMed: 8837884]
2. McMinn PC. An overview of the evolution of enterovirus 71 and its clinical and public health significance. FEMS Microbiol Rev. 2002; 26:91–107. [PubMed: 12007645]
3. Wu Y, et al. Structures of EV71 RNA-dependent RNA polymerase in complex with substrate and analogue provide a drug target against the hand-foot-and- mouth disease pandemic in China. Protein Cell. 2010; 1:491–500. [PubMed: 21203964]

4. Basavappa R, et al. Role and mechanism of the maturation cleavage of VP0 in poliovirus assembly: structure of the empty capsid assembly intermediate at 2.9 A resolution. Protein Sci. 1994; 3:1651–69. [PubMed: 7849583]
5. Curry S, et al. Dissecting the roles of VP0 cleavage and RNA packaging in picornavirus capsid stabilization: the structure of empty capsids of foot-and- mouth disease virus. J Virol. 1997; 71:9743–52. [PubMed: 9371640]
6. Tuthill TJ, Groppelli E, Hogle JM, Rowlands DJ. Picornaviruses. Cell Entry by Non-Enveloped Viruses. 2010; 343:43–89.
7. Ansardi DC, Morrow CD. Amino acid substitutions in the poliovirus maturation cleavage site affect assembly and result in accumulation of provirions. J Virol. 1995; 69:1540–7. [PubMed: 7853487]
8. Jacobson MF, Baltimore D. Morphogenesis of poliovirus. I. Association of the viral RNA with coat protein. J Mol Biol. 1968; 33:369–78. [PubMed: 4302632]
9. Liu CC, et al. Purification and characterization of enterovirus 71 viral particles produced from vero cells grown in a serum-free microcarrier bioreactor system. PLoS One. 2011; 6:e20005. [PubMed: 21603631]
10. Guttman N, Baltimore D. A plasma membrane component able to bind and alter virions of poliovirus type 1: studies on cell-free alteration using a simplified assay. Virology. 1977; 82:25–36. [PubMed: 197703]
11. Marongiu ME, Pani A, Corrias MV, Sau M, La Colla P. Poliovirus morphogenesis. I. Identification of 80S dissociable particles and evidence for the artifactual production of procapsids. J Virol. 1981; 39:341–7. [PubMed: 6268826]
12. Le Bouvier GL. The modification of poliovirus antigens by heat and ultraviolet light. Lancet. 1955; 269:1013–6. [PubMed: 13272322]
13. Blondel B, Akacem O, Crainic R, Couillin P, Horodniceanu F. Detection by monoclonal antibodies of an antigenic determinant critical for poliovirus neutralization present on VP1 and on heat-inactivated virions. Virology. 1983; 126:707–10. [PubMed: 6190311]
14. Hogle JM. Poliovirus cell entry: common structural themes in viral cell entry pathways. Annu Rev Microbiol. 2002; 56:677–702. [PubMed: 12142481]
15. Olson NH, et al. Structure of a Human Rhinovirus Complexed with Its Receptor Molecule. Proc Natl Acad Sci U S A. 1993; 90:507–511. [PubMed: 8093643]
16. Rossmann MG, et al. Structure of a human common cold virus and functional relationship to other picornaviruses. Nature. 1985; 317:145–53. [PubMed: 2993920]
17. Zhang P, et al. Crystal structure of CD155 and electron microscopic studies of its complexes with polioviruses. Proc Natl Acad Sci U S A. 2008; 105:18284–9. [PubMed: 19011098]
18. Crowell RL, Philipson L. Specific alterations of coxsackievirus B3 eluted from HeLa cells. J Virol. 1971; 8:509–15. [PubMed: 4331654]
19. Kaplan G, et al. Identification of a surface glycoprotein on African green monkey kidney cells as a receptor for hepatitis A virus. EMBO J. 1996; 15:4282–96. [PubMed: 8861957]
20. Lonberg-Holm K, Gosser LB, Kauer JC. Early alteration of poliovirus in infected cells and its specific inhibition. J Gen Virol. 1975; 27:329–42. [PubMed: 167116]
21. Fricks CE, Hogle JM. Cell-induced conformational change in poliovirus: externalization of the amino terminus of VP1 is responsible for liposome binding. J Virol. 1990; 64:1934–45. [PubMed: 2157861]
22. Greve JM, et al. Mechanisms of receptor-mediated rhinovirus neutralization defined by two soluble forms of ICAM-1. J Virol. 1991; 65:6015–23. [PubMed: 1681115]
23. Bostina M, Levy H, Filman DJ, Hogle JM. Poliovirus RNA is released from the capsid near a twofold symmetry axis. J Virol. 2011; 85:776–83. [PubMed: 20980499]
24. Bubeck D, et al. The structure of the poliovirus 135S cell entry intermediate at 10-angstrom resolution reveals the location of an externalized polypeptide that binds to membranes. J Virol. 2005; 79:7745–55. [PubMed: 15919927]
25. Levy HC, Bostina M, Filman DJ, Hogle JM. Catching a virus in the act of RNA release: a novel poliovirus uncoating intermediate characterized by cryo-electron microscopy. J Virol. 2010; 84:4426–41. [PubMed: 20181687]

26. Hendry E, et al. The crystal structure of coxsackievirus A9: new insights into the uncoating mechanisms of enteroviruses. Structure. 1999; 7:1527–38. [PubMed: 10647183]
27. Belnap DM, et al. Molecular tectonic model of virus structural transitions: the putative cell entry states of poliovirus. J Virol. 2000; 74:1342–54. [PubMed: 10627545]
28. Siebert X, Navaza J. UROX 2.0: an interactive tool for fitting atomic models into electron-microscopy reconstructions. Acta Crystallogr D Biol Crystallogr. 2009; 65:651–8. [PubMed: 19564685]
29. Filman DJ, et al. Structural factors that control conformational transitions and serotype specificity in type 3 poliovirus. EMBO J. 1989; 8:1567–79. [PubMed: 2548847]
30. Grant RA, et al. Structures of poliovirus complexes with anti-viral drugs: implications for viral stability and drug design. Curr Biol. 1994; 4:784–97. [PubMed: 7820548]
31. Smith TJ, et al. The site of attachment in human rhinovirus 14 for antiviral agents that inhibit uncoating. Science. 1986; 233:1286–93. [PubMed: 3018924]
32. McSharry JJ, Caliguiri LA, Eggers HJ. Inhibition of uncoating of poliovirus by arildone, a new antiviral drug. Virology. 1979; 97:307–15. [PubMed: 224584]
33. Hogle JM, Chow M, Filman DJ. Three-dimensional structure of poliovirus at 2.9 A resolution. Science. 1985; 229:1358–65. [PubMed: 2994218]
34. Smyth M, et al. Implications for viral uncoating from the structure of bovine enterovirus. Nat Struct Biol. 1995; 2:224–31. [PubMed: 7773791]
35. Foo DG, et al. Identification of neutralizing linear epitopes from the VP1 capsid protein of Enterovirus 71 using synthetic peptides. Virus Res. 2007; 125:61–8. [PubMed: 17222936]
36. Liu CC, et al. Identification and characterization of a cross-neutralization epitope of Enterovirus 71. Vaccine. 2011; 29:4362–72. [PubMed: 21501643]
37. Yang SL, Chou YT, Wu CN, Ho MS. Annexin II Binds to Capsid Protein VP1 of Enterovirus 71 and Enhances Viral Infectivity. J Virol. 2011; 85:11809–20. [PubMed: 21900167]
38. Nishimura Y, et al. Human P-selectin glycoprotein ligand-1 is a functional receptor for enterovirus 71. Nat Med. 2009; 15:794–7. [PubMed: 19543284]
39. Yamayoshi S, et al. Scavenger receptor B2 is a cellular receptor for enterovirus 71. Nat Med. 2009; 15:798–801. [PubMed: 19543282]
40. Rossmann MG, He Y, Kuhn RJ. Picornavirus-receptor interactions. Trends Microbiol. 2002; 10:324–31. [PubMed: 12110211]
41. He Y, et al. Complexes of poliovirus serotypes with their common cellular receptor, CD155. J Virol. 2003; 77:4827–35. [PubMed: 12663789]
42. Xiao C, et al. The crystal structure of coxsackievirus A21 and its interaction with ICAM-1. Structure. 2005; 13:1019–33. [PubMed: 16004874]
43. Oliveira MA, et al. The structure of human rhinovirus 16. Structure. 1993; 1:51–68. [PubMed: 7915182]
44. Kim S, et al. Conformational variability of a picornavirus capsid: pH-dependent structural changes of Mengo virus related to its host receptor attachment site and disassembly. Virology. 1990; 175:176–90. [PubMed: 2155508]
45. McDermott BM Jr. Rux AH, Eisenberg RJ, Cohen GH, Racaniello VR. Two distinct binding affinities of poliovirus for its cellular receptor. J Biol Chem. 2000; 275:23089–96. [PubMed: 10770940]
46. Giranda VL, et al. Acid-induced structural changes in human rhinovirus 14: possible role in uncoating. Proc Natl Acad Sci U S A. 1992; 89:10213–7. [PubMed: 1332036]
47. Davis MP, et al. Recombinant VP4 of human rhinovirus induces permeability in model membranes. J Virol. 2008; 82:4169–74. [PubMed: 18256154]
48. Racaniello VR. Early events in poliovirus infection: virus-receptor interactions. Proc Natl Acad Sci U S A. 1996; 93:11378–81. [PubMed: 8876143]
49. Lin J, et al. An externalized polypeptide partitions between two distinct sites on genome-released poliovirus particles. J Virol. 2011; 85:9974–83. [PubMed: 21775460]

50. Kay BK, Williamson MP, Sudol M. The importance of being proline: the interaction of proline-rich motifs in signaling proteins with their cognate domains. FASEB J. 2000; 14:231–41. [PubMed: 10657980]

51. Stuart DI, Levine M, Muirhead H, Stammers DK. Crystal structure of cat muscle pyruvate kinase at a resolution of 2.6 A. J Mol Biol. 1979; 134:109–42. [PubMed: 537059]

52. Walter TS, et al. A procedure for setting up high-throughput nanolitre crystallization experiments. Crystallization workflow for initial screening, automated storage, imaging and optimization. Acta Crystallogr D Biol Crystallogr. 2005; 61:651–7. [PubMed: 15930615]

53. Otwinowski Z, Borek D, Cymborowski M, Machius M, Minor W. Diffraction data analysis in the presence of radiation damage. Acta Crystallographica D Bioll Crystallogr. 2010; 66:426–436. [PubMed: 20382996]

54. Brunger AT, et al. Crystallography & NMR system: A new software suite for macromolecular structure determination. Acta Crystallogr D Biol Crystallogr. 1998; 54:905–21. [PubMed: 9757107]

55. Emsley P, Lohkamp B, Scott WG, Cowtan K. Features and development of Coot. Acta Crystallogr D Biol Crystallogr. 2010; 66:486–501. [PubMed: 20383002]

56. Blanc E, et al. Refinement of severely incomplete structures with maximum likelihood in BUSTER-TNT. Acta Crystallogr D Biol Crystallogr. 2004; 60:2210–21. [PubMed: 15572774]

57. Laskowski RA, Moss DS, Thornton JM. Main-chain bond lengths and bond angles in protein structures. J Mol Biol. 1993; 231:1049–67. [PubMed: 8515464]

58. DeLano WL. The PyMOL Molecular Graphics System. 2002

Europe PMC Funders Author Manuscripts

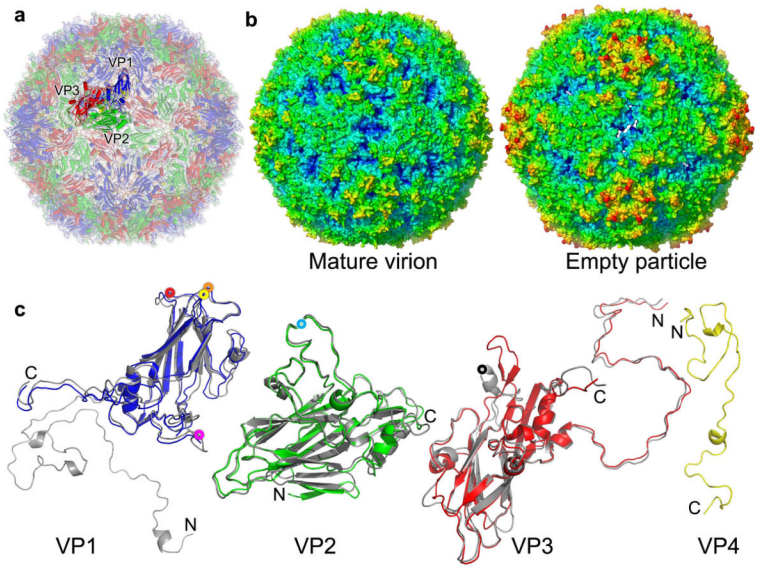

Figure 1.

Overall structures. (**a),** Cartoon of the mature EV71 virion, looking down an icosahedral 2-fold axis; VP1, VP2, VP3 and VP4 are drawn in blue, green, red and yellow, respectively. A single icosahedral protomer is drawn more brightly. (**b),** Radius colored surface representation of EV71 mature and empty particles. The surfaces for both are colored from blue to red according to their distances from the particle center. (**c),** Structures of the EV71 capsid proteins. VP0-3 (we treat VP0 and VP2 interchangeably) are shown in a similar orientation to the brighter protomer in **(a)**; proteins from the expanded empty particle are coloured as in **(a),** whereas the corresponding chains from the mature virion are grey. VP4 of the mature virion is shown in yellow. The proteins have been superimposed as rigid bodies (216, 227, 220 Cαs superpose with rms deviations of 1.6, 0.9 and 1.3Å for VP1, VP0(2) and VP3 respectively). Residues 1-297 of VP1, 10-254 of VP2, 1-242 of VP3 and 12-69 of VP4 have well defined electron density in the mature virion, while residues 73-210 and 219-297 of VP1, 82-319 of VP0 and 1-238 of VP3 in the empty particle are modeled. Major surface exposed loops are marked with coloured washers: VP1 BC (yellow), VP1 DE (orange), VP1 HI (red), VP1 GH (magenta), VP2 EF (light blue), VP3 GH (black).

Europe PMC Funders Author Manuscripts

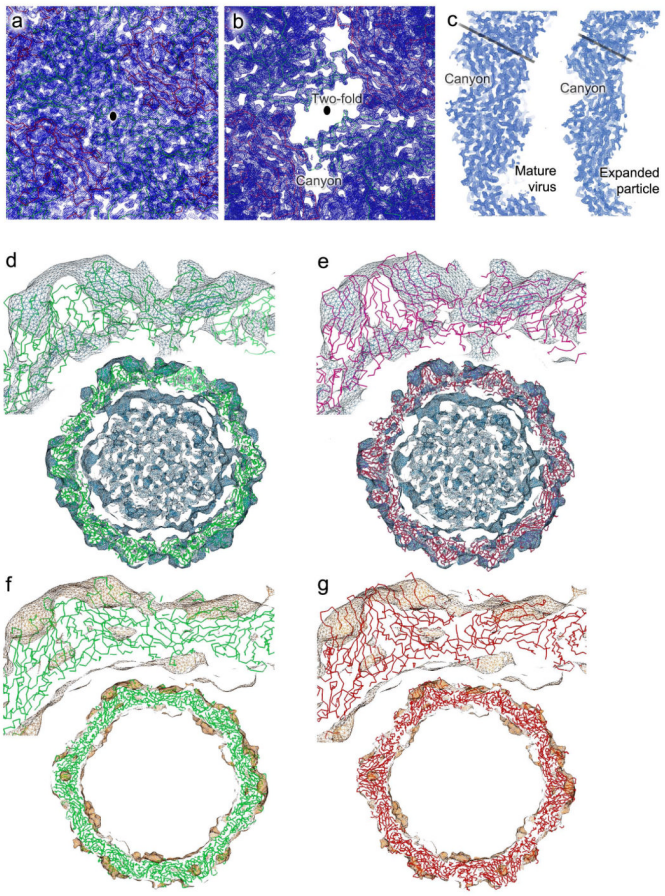

Figure 2.

Electron density. **(a)** and **(b):** averaged $2|F|_o-|F_c|$ maps in the vicinity of an icosahedral 2-fold axis (marked as black ellipse) for the mature virus (**a**) and expanded particle (**b**), showing the well defined electron density and demonstrating the perforations in the expanded particle. Cα traces, coloured as in Fig. 1 are also shown. **(c)**, Equivalent equatorial slices through the two electron density maps shown in **(a)** and **(b)**. The black lines mark the approximate position of an icosahedral 5-fold axis. **(d-g)** Comparisons of the fit of our crystallographic EV71 expanded particle coordinates and modeled poliovirus into the 10 Å resolution cryo-EM reconstructions for 135S and 82S poliovirus particles[24,25]. The density was displayed and correlation coefficients calculated using the program URO[28]. **(d)** and **(e)** show the fit of EV71 (green) and poliovirus (red) into the density for the 135S particle (correlation coefficient 0.66 for both EV71 and the deposited poliovirus coordinates). (**f**) and (**g**) show the corresponding fits into the cryo-EM density for the late 80S poliovirus (correlation coefficients 0.63 for EV71 and 0.64 for poliovirus).

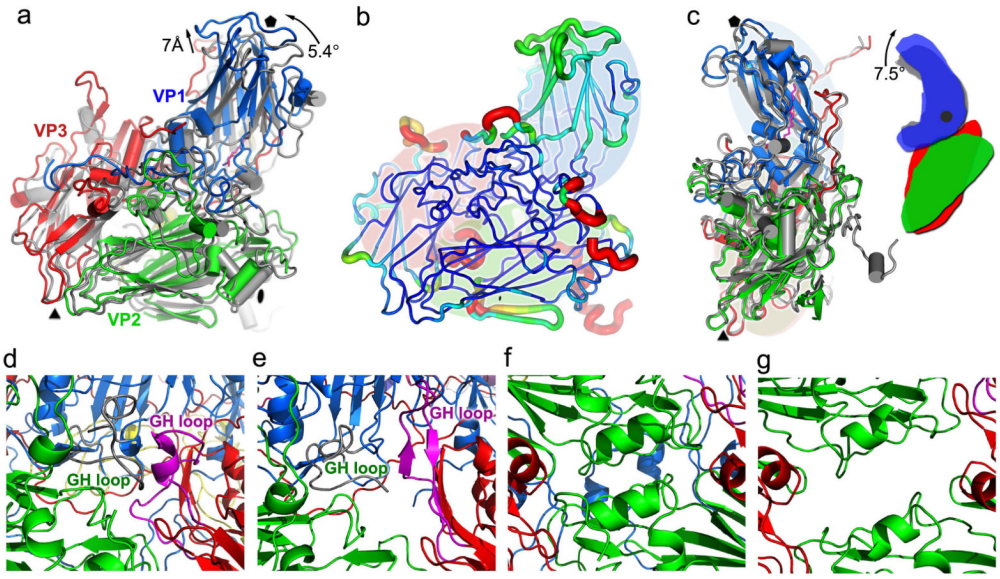

Figure 3.

Protomers of mature virion and expanded particle compared. **(a)**, protomeric units shown with respect to the icosahedral axes of the particles (*i.e.* superposing whole particles). The mature virus is grey and the expanded particle coloured as in Figure 1c. The orientation is similar to the bright protomer in Figure 1a, icoshedral symmetry axes are drawn in black. **(b),** Superposed protomers[51]. Structural differences are mapped onto the protomer of the mature virion, the thickness and colour of the worm representation reflects the local deviation between the structures (ramped blue 0 to orange 8Å). Regions missing in the expanded particle are shown in red (VP4 is omitted). **(c),** the change in the jackknife structure of VP1 on capsid expansion. The superposition is based on VP0(2), VP3 and the 5-fold distal portion of VP1. Black dot in the right diagram marks the point about which VP1 flexes. (**d)-(g**) show the regions where perforations appear in the expanded particle (the base of the canyon in **(d)** and **(e)** and the 2-fold region in **(f)** and **(g),** the mature virus is on the left and expanded particle on the right). **(c)-(g)** coloured as in Figure 1c, with the GH loops of VP1 and VP3 highlighted in grey and magenta, respectively. Residues 136-141 of VP3 and 227-250 and 48-52 of VP2 form a bridge separating the perforations.

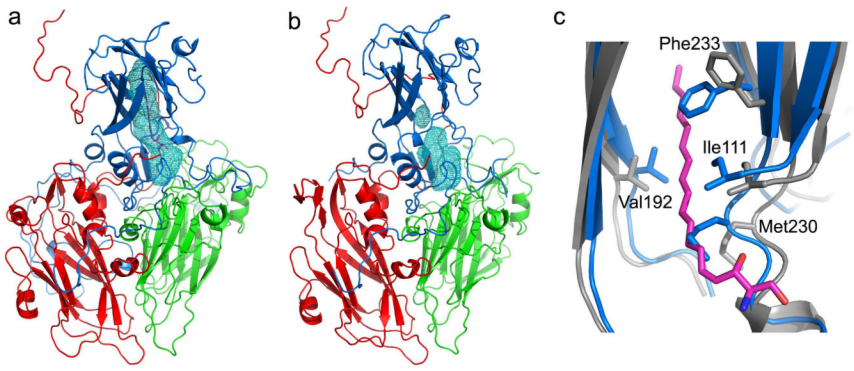

Figure 4.

Pocket factor binding site. **(a)**, VP1 of EV71 mature virus harbours a hydrophobic pocket (blue mesh) similar to that seen in other enteroviruses, which is occupied by a natural lipid, probably sphingosine (magenta). The protein cartoon is coloured as for Figure 1a. **(b)**, The expanded particle, showing the collapsed pocket. **(c)**, Comparison of the VP1 pockets between the mature virus (grey, with pocket factor shown in magenta) and empty particles (blue). During pocket collapse residues 110-114, 152- 160, 190-194 and 228-234 move inwards taking some internal hydrophobic residues with them (including I111, F135 and F155).

Europe PMC Funders Author Manuscripts

Table 1

Data collection, phasing and refinement statistics

	Formaldehyde inactivated				Non-inactivated particles	
	Mature virus	**Mature virus**	**Empty particle**	**Empty particle**	**Mature virus**	**Empty particle**
Data collection						
Temperature (K)	293	293	293	100	293	293
No. crystals (positions)	45 (94)	76(98)	17(39)	3(3)	45(50)	41(55)
Wavelength (Å)	0.9686	0.96860	0.96860	0.9750	0.9686	0.9686
Space group	*R32*	*I23*	$P4_232$	$P4_232$	*I23*	$P4_232$
Cell dimensions						
a, *b*, *c* (Å)	*a*=*b*=330.0, *c*=748.4	*a*=*b*=*c*=600.1	*a*=*b*=*c*=354.9	*a*=*b*=*c*=353.1	*a*=*b*=*c*=599.8	*a*=*b*=*c*=355.9
Resolution (Å)	50.0–2.30 (2.38–2.30)	50.0–2.60 (2.69–2.60)	50.0–3.80 (3.94–3.80)	50.0–2.88 (2.98–2.88)	50.0–3.00 (3.11–3.00)	50.0–4.00 (4.14–4.00)
Unique reflections	405370(10180)	918888(40599)	69774(6944)	167672(16211)	612286(59348)	64534(6338)
R_{merge}	0.377	0.576	0.437	0.382	0.680	0.386
$I / \sigma I$	1.9(0.5)	1.3(0.3)	2.1(0.5)	6.0(1.2)	1.2(0.5)	1.9(0.7)
Completeness (%)	59.1(14.9)	84.8(37.6)	92.6(93.8)	99.6(97.7)	86.8(84.5)	99.2(99.4)
Redundancy	2.2(1.1)	2.9(1.7)	3.1(3.2)	23.5(20.1)	2.4(2.2)	6.0(6.0)
Refinement						
Resolution (Å)	50.0 – 2.30	50.0 – 2.60	50.0 – 3.80	50.0 – 2.88	50.0 – 3.00	50.0 – 4.00
No. reflections	389853/3978	868691/8680	67198/675	167479/1685	597914/6030	63598/641
R_{work} /R_{free} *	0.217/0.226	0.236/0.240	0.257/0.284	0.227/0.234	0.272/0.283	0.272/0.278
No. atoms						
Protein	6508	6508	5397	5397	6508	5397
Water/other	220	330		69	21	
B-factors						
Main chain	23	25	111	64	22	109
Other atoms	25	28	112	65	23	110
R.m.s. deviations						
Bond lengths (Å)	0.011	0.011	0.009	0.011	0.009	0.011
Bond angles (°)	1.7	1.6	1.5	1.6	1.5	1.6

Europe PMC Funders Author Manuscripts

* Note that the R_{free} is of limited significance owing to the considerable non-crystallographic symmetry.